J Mater Sci (2009) 44:5732–5736
DOI 10.1007/s10853-009-3802-3

Crystal structure and methane oxidation on perovskite-type $(La_{1-x}Nd_x)CoO_3$ synthesized using citric acid

Hideki Taguchi · Sho Matsuoka · Masaki Kato · Ken Hirota

Received: 8 June 2009 / Accepted: 8 August 2009 / Published online: 27 August 2009

Abstract Perovskite-type $(La_{1-x}Nd_x)CoO_3$ was synthesized using citric acid at 700 °C. The Rietveld method indicated that the crystal structure changed from a rhombohedral to an orthorhombic system at $x = 0.4$. The Co–O distance of the rhombohedral structure connected continuously with the average Co–O(2) distance of the orthorhombic structure, and the Co–O–Co angle of the rhombohedral structure and the Co–O(2)–Co angle of the orthorhombic structure were continuous. The average particle size of the samples was approximately 55 nm. CH_4 oxidation started above 300 °C, and the temperature corresponding to the 50% conversion ($T_{1/2}$) of CH_4 increased linearly with increases in x. It is considered that the amount of adsorbed oxygen decreased in response to the steric hindrance, and that $T_{1/2}$ increased as a result.

Introduction

It is well known that perovskite-type oxides (ABO_3) provide excellent catalysis of hydrocarbon (C_nH_{2n+2}) oxidation [1–10]. It is important to develop a new, alternative catalyst for CH_4 oxidation. The catalytic activity of perovskite-type oxides in CH_4 oxidation is essentially controlled by the B-site cation and is improved by the substitution of another A-site or B-site cation [1, 4–6]. Since CH_4 oxidation occurs on the outmost surface of the catalyst, it is necessary to synthesize perovskite-type oxides with good surface crystallinity (regularity of ions) and/or a large specific surface area.

Perovskite-type $LaMO_3$ (M = Mn, Co) has been known to show high catalytic activity in carbon monoxide (CO) oxidation [1, 8]. Although $LaMO_3$ (M = Mn, Co) synthesized using poly(acrylic acid) (PAA) has a large specific surface area, the rapid combustion of PAA causes cracks on the catalytic surface [11–13]. In order to reduce the number of cracks and improve the surface crystallinity, a gel was prepared by adding citric acid to an aqueous solution of metal nitrates [14, 15]. The resulting $LaCoO_3$ synthesized using citric acid was found to have higher catalytic activity for CO oxidation [15]. Recently, Yi et al. prepared highly crystalline $LaCoO_3$ using a novel microwave-assisted process with a La–Co citrate complex precursor in the host pores of mesoporous silica [6]. According to Natile et al. [16], two nanostructured $LaCoO_3$ were prepared with co-precipitation and with the citrate gel method. X-ray powder diffraction pattern indicated that only the sample prepared with the citrate gel method provided a single phase. The results of X-ray photoelectron spectroscopy and diffusion reflection infrared Fourier transform spectroscopy suggested that the sample prepared with the citrate gel method had a low presence of hydroxyl groups and carbonate species. Nano-sized $LaCoO_3$ powder was successfully prepared by an aqueous gel-casting method, and the effect of the ratio of organic precursors to metal nitrates and the ratio of acrylamide (AM) and *N,N′*-methylenebisacrylamide (MBAM) were investigated [17]. The particle size of the nano-powders was 31–60 nm and decreased with increasing the ratio of organic precursor to metal nitrates but was not affected by the ratio of AM to MBAM.

H. Taguchi (✉)
The Graduate School of Natural Science and Technology (Science), Okayama University, 3-1-1 Tsushima-naka, Okayama 700-8530, Japan
e-mail: htaguchi@cc.okayama-u.ac.jp

S. Matsuoka · M. Kato · K. Hirota
Department of Molecular Chemistry and Biochemistry, Faculty of Science and Engineering, Doshisha University, Kyo-Tanabe, Kyoto 610-0321, Japan

There have been many reports regarding hydrocarbon oxidation of the perovskite-type oxide that results in changes in the kind of B-site cation or the valence of the B-site cation [1, 2, 4–6, 18–21]. Saracco et al. have reported that $La(Cr_{1-x}Mg_x)O_3$ promotes CH_4 oxidation in proportion to Mg/Cr substitution [2]. According to Arai et al. [18], $(La_{1-x}A_x)MO_3$ (A = Sr, Ca, Ba; M = Mn, Fe, Co) shows high CH_4 oxidation, and the reaction kinetics can be explained by assuming CH_4 oxidation occurs by means of parallel reactions involving both adsorbed oxygen and lattice oxygen. To the best of our knowledge, there have been no articles regarding the effects of the crystal structure of the perovskite-type oxides on CH_4 oxidation. In this study, perovskite-type $(La_{1-x}Nd_x)CoO_3$ was synthesized using the polymerizable complex method. We then examined the relationship between the crystal structure of the perovskite-type oxides and the catalytic activity of these oxides in CH_4 oxidation based on determination of the crystal structure and measurement of the average particle size and catalysis.

Experimental

High-purity powders of lanthanum nitrate hexahydrate (Nacalai Tesque, Japan, 99.9%), neodymium nitrate hexahydrate (Kanto Kagaku, Japan, 99.95%), and cobalt acetate tetrahydrate (Nacalai Tesque, Japan, 99.0%) were weighed to the desired proportions. A small amount of nitric acid and distilled water was added to dissolve the powders. Citric acid (CA, Kanto Kagaku, Japan, 99.5%) was then added to make the gel, resulting in a molar ratio of (La + Nd): Co:CA = 1:1:1. The solution was left to sit for 12 h at 120 °C until it had gelled. The gel was slowly heated to 700 °C for 3 h in air. The heating rate was 7.5 °C/min.

The oxygen content of the sample was determined by iodometry. After potassium iodide solution and hydrochloric acid had been added to dissolve the sample in a beaker, the solution was titrated with a standard thiosulfate solution [22]. The crystal phase of the sample was identified by powder X-ray diffraction (XRD, Model RAD-1C, RIGAKU, Japan) using monochromatic CuKα radiation. The structural refinement was carried out by the Rietveld method with XRD data [23]. The XRD data at room temperature were collected by step scanning over an angular range of $20° \leq 2\theta \leq 100°$ in increments of 0.02° (2θ). The average particle size of the sample was measured by transmission electron microscopy (TEM, Model JEM2100F, JEOL, Japan). The catalytic activity of CH_4 oxidation was measured as follows. The sample (0.20 g) was preheated at 300 °C in air. A mixed gas of CH_4 (3.0%), O_2 (6.0%), and He (balance) was fed into a flow reactor at a flow rate of 7.5×10^{-5} m^3/min. The space velocity was approximately 11,000 h^{-1} in all measurements. The product was analyzed by gas chromatography (Model D-2500, HITACHI, Japan) using a column (molecular sieve 13×) kept at 50 °C during the measurement.

Results and discussion

The oxygen content of all $(La_{1-x}Nd_x)CoO_3$ synthesized using citric acid was determined to be 3.00 ± 0.02 from iodometry and was independent of x. The XRD patterns of the samples at room temperature were completely indexed as a rhombohedral perovskite-type structure in the range of $0 \leq x \leq 0.3$ and as an orthorhombic perovskite-type structure in the range of $0.4 \leq x \leq 1.0$. Structural refinement was carried out by the Rietveld method to determine the Co–O distance and the Co–O–Co angle of the samples. In this study, we assumed the space groups of the rhombohedral and orthorhombic structures to be $R\bar{3}c$ and *Pnma*, respectively [24, 25]. Tables 1 and 2 show the refined structural parameters of the samples. R_{WP}, R_I, and R_F are the weighted pattern, the integrated R factor, and the structure factor, respectively. The R_{WP} of all samples was less than 10.63%. The observed XRD pattern of $(La_{0.8}Nd_{0.2})CoO_{3.0}$ ($x = 0.2$) agreed very well with that obtained by the simulation, as shown in Fig. 1. The lattice constant (a) of the rhombohedral structure decreased monotonously with

Table 1 The refined structural parameters and the tolerance factor (t) of rhombohedral perovskite-type $(La_{1-x}Nd_x)CoO_3$

	$x = 0.0$	$x = 0.1$	$x = 0.2$	$x = 0.3$
Cell data				
a (Å)	5.3793 (5)	5.3731 (6)	5.3636 (6)	5.3570 (8)
α (°)	60.77 (1)	60.78 (1)	60.83 (1)	60.80 (1)
V (Å^3)	111.97 (2)	111.61 (2)	111.14 (2)	110.67 (3)
R factor (%)				
R_{WP}	9.69	8.34	8.90	10.63
R_I	0.94	1.38	1.49	1.62
R_F	0.72	0.97	1.02	1.10
Atomic parameters[a]				
La,Nd				
B (Å^2)	0.49 (2)	0.55 (2)	0.53 (2)	0.61 (2)
Co				
B (Å^2)	0.18 (3)	0.26 (3)	0.26 (3)	0.24 (3)
O				
x	−0.203 (1)	−0.201 (1)	−0.199 (1)	−0.198 (1)
B (Å^2)	0.70 (8)	0.83 (8)	0.81 (9)	1.08 (11)
t	0.991	0.987	0.984	0.981

[a] *Atomic position*: La,Nd (2*a*) 1/4, 1/4, 1/4: Co (2*b*) 0, 0, 0: O (6*e*) $-x$, $x + 1/2$, 1/4

Table 2 The refined structural parameters and the tolerance factor (t) of orthorhombic perovskite-type $(La_{1-x}Nd_x)CoO_3$

	$x = 0.4$	$x = 0.5$	$x = 1.0$
Cell data			
a (Å)	5.3587 (2)	5.3562 (2)	5.3360 (2)
b (Å)	7.6096 (3)	7.6028 (4)	7.5521 (5)
c (Å)	5.4138 (2)	5.4044 (2)	5.3481 (3)
V (Å^3)	220.76 (1)	220.08 (2)	215.52 (2)
R factor (%)			
R_{WP}	9.14	9.47	10.39
R_I	1.41	1.77	1.62
R_F	1.33	1.85	1.41
Atomic parameters[a]			
La,Nd			
x	0.019 (1)	0.021 (1)	0.034 (1)
z	0.006 (1)	0.006 (1)	−0.006 (1)
B (Å^2)	0.54 (2)	0.58 (2)	0.52 (2)
Co			
B (Å^2)	0.25 (3)	0.29 (3)	0.21 (3)
O(1)			
x	0.500 (1)	0.498 (1)	0.492 (1)
z	−0.028 (2)	−0.029 (3)	0.070 (3)
B (Å^2)	2.75 (46)	3.94 (63)	1.24 (51)
O(2)			
x	0.267 (1)	0.271 (2)	0.280 (2)
y	0.467 (1)	0.466 (1)	0.462 (1)
z	−0.275 (1)	−0.278 (1)	−0.288 (2)
B (Å^2)	0.89 (21)	0.46 (24)	0.22 (27)
t	0.978	0.975	0.958

[a] *Atomic position*: La,Nd (4*c*) *x*, 1/4, *z*: Co (4*b*) 0, 0, 1/2: O(1) (4*c*) *x*, 1/2, *z*: O(1) (8*d*) *x*, *y*, *z*

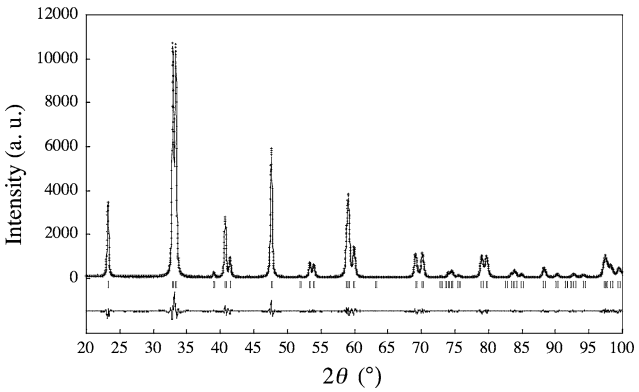

Fig. 1 Observed XRD and the difference between the observation and calculation of $(La_{0.8}Nd_{0.2})CoO_{3.0}$ ($x = 0.2$)

increases in x, as shown in Table 1. The lattice constants (a, b, and c) of the orthorhombic structure also decreased monotonously with increases in x, as shown in Table 2. The present values of $LaCoO_3$ and $NdCoO_3$ were nearly equal to the reported values [24, 25]. The coordination number of the La^{2+} and Nd^{3+} ions is 12, and that of the Co ion is 6 in the perovskite-type structure. The ionic radii of the La^{3+}, Nd^{3+}, low-spin Co^{3+}, and high-spin Co^{3+} ions are 1.36 Å, 1.27 Å, 0.545 Å, and 0.61 Å, respectively [26]. Therefore, the decrease in the lattice constants can be explained by the difference between the ionic radius of the La^{3+} ion and that of the Nd^{3+} ion. Mastin et al. discussed the deviation of the crystal structure of $(La_{1-x}Ca_x)CoO_3$ from cubic symmetry using the tolerance factor [27]. Although the tolerance factor of $(La_{1-x}Ca_x)CoO_3$ increased with increases in the Ca^{2+} ion content, the tolerance factor of this system decreased with increases in the Nd^{3+} ion content as shown in Tables 1 and 2. The results indicated that the decrease of the tolerance factor corresponded to the transition of the crystal structure of $(La_{1-x}Nd_x)CoO_3$.

The A-site cation (La or Nd ions) coordinates with 12 O ions in the rhombohedral structure, and the B-site cation (Co ion) coordinates with 6 O ions [24]. In contrast, the A-site cation (La ion) coordinates with 12 anions in the orthorhombic structure [28]: 4 O(1) and 8 O(2) ions. The B-site cation (Co ion) coordinates with 6 anions: 2 O(1) and 4 O(2) ions. The O(1) ion bonds with the Co ion along the b-axis, and the O(2) ion bonds with the Co ion along the a-axis and c-axis. Figure 2 shows the relationship between the Co–O distance and x. The Co–O distance of the rhombohedral structure decreased linearly with increases in x. The Co–O(1) distance of the orthorhombic structure distance increased with increases in x, but the Co–O(2) distances remained constant. The average Co–O(2) distance was approximately 1.928 Å, and this value corresponded closely to the value of $x = 0.3$. Figure 3 shows the relationship between the Co–O–Co angle and x. The Co–O–Co angle of the rhombohedral structure decreased linearly with

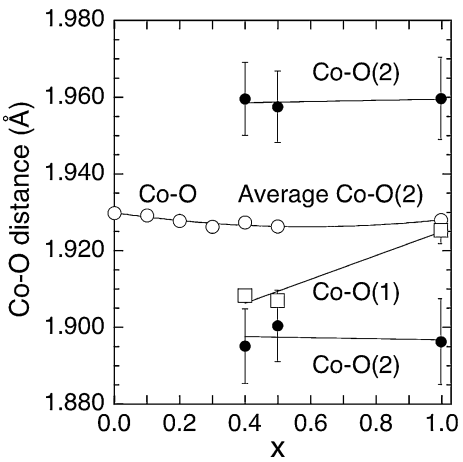

Fig. 2 The relationship between the Co–O distance of $(La_{1-x}Nd_x)CoO_3$ and x

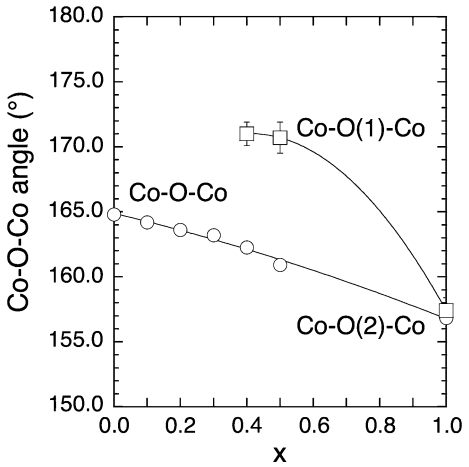

Fig. 3 The relationship between the Co–O–Co angle of $(La_{1-x}Nd_x)CoO_3$ and x

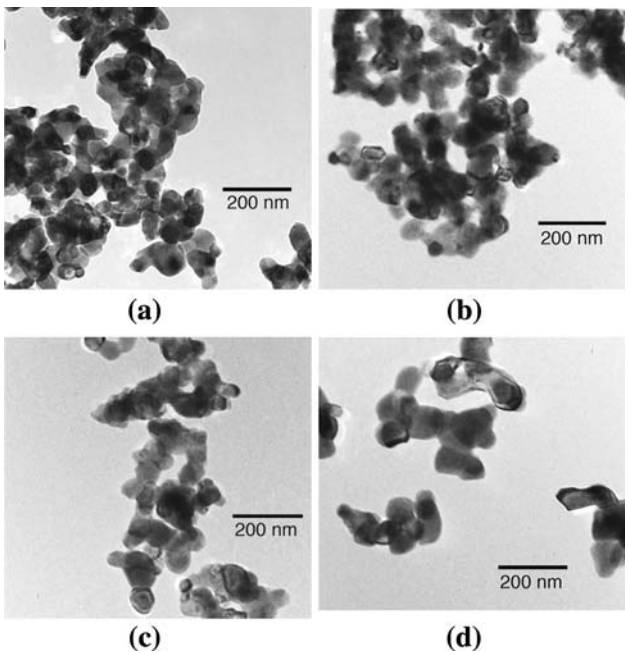

Fig. 4 TEM photographs of $(La_{1-x}Nd_x)CoO_3$. **a** $x = 0.0$, **b** $x = 0.2$, **c** $x = 0.4$, **d** $x = 1.0$

increases in x. Although both the Co–O(1)–Co and Co–O(2)–Co angles of the orthorhombic structure also decreased with increases in x, the variations in the Co–O(2)–Co and Co–O–Co angles of the rhombohedral structure were continuous.

Figure 4 shows the TEM photographs of $(La_{1-x}Nd_x)CoO_3$ ($x = 0.0$, 0.2, 0.4, and 1.0). The particles of the samples did not show a distinct shape, and the average particle size determined from the TEM observation was independent of x: 52 ± 6 nm ($x = 0.0$), 55 ± 8 nm ($x = 0.2$), 57 ± 8 nm ($x = 0.4$), and 55 ± 7 nm ($x = 1.0$). Figure 5 shows the relationship between the conversion of

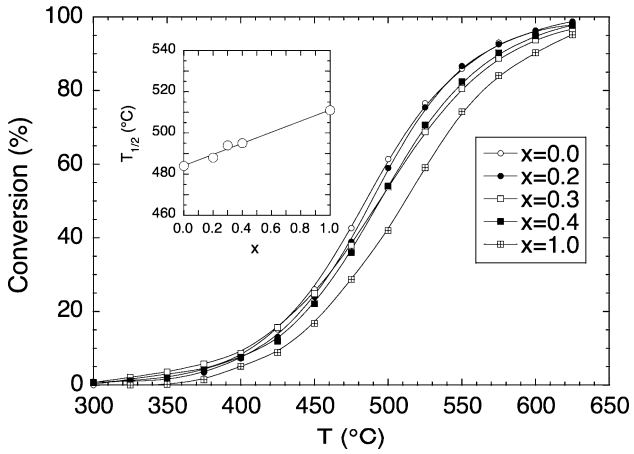

Fig. 5 The relationship between the conversion of CH_4 on $(La_{1-x}Nd_x)CoO_3$ and x. The inset is the relationship between the 50% conversion ($T_{1/2}$) and x

CH_4 on $(La_{1-x}Nd_x)CoO_3$ and x. CH_4 oxidation started above 300 °C. The catalytic activity of a given catalyst is usually expressed in terms of the temperature corresponding to the 50% conversion ($T_{1/2}$) of CH_4, which can be obtained from the conversion versus temperature curve [29]. The relationship between $T_{1/2}$ and x is inset in Fig. 5. $T_{1/2}$ increased linearly with increases in x: 484 °C for $x = 0.0$, 488 °C for $x = 0.2$, 494 °C for $x = 0.3$, 495 °C for $x = 0.4$, and 511 °C for $x = 1.0$. According to Arai et al. [18], $T_{1/2}$ of CH_4 oxidation on $LaCoO_3$ synthesized by decomposition of metal acetates at 850 °C is 525 °C. Yi et al. have reported that $T_{1/2}$ of CH_4 oxidation on $LaCoO_3$ using a novel microwave-assisted process is approximately 500 °C [6]. These values are higher than the $T_{1/2}$ of this study.

Voorhoeve et al. have reported that CO oxidation occurs at the metal ion of the surface [30]. CO_2 is produced by the reaction of CO with oxygen adsorbed on the metal ions of the outmost surface, and the amount of adsorbed oxygen depends on the valence of the metal ion, the amount of the metal ion, and the surface crystallinity (regularity of ions) [14]. Seyfi et al. reported that the catalytic activity of the perovskite samples depends on three factors; chemical composition, degree of crystallinity, and the crystals morphology [9]. In this study, $(La_{1-x}Nd_x)CoO_3$ had a stoichiometric composition, and the average particle size of the samples was approximately 55 nm. These results indicated that the valence of the Co ion was 3+ in the range of $0.0 \leq x \leq 1.0$, and that the specific surface area of the sample remained nearly constant because the particle size was constant. Although the crystal structure of the sample changed at $x = 0.4$, the Co–O distance of the rhombohedral structure and the average Co-O(2) distance of the orthorhombic structure were continuous. The Co–O–Co angle of the rhombohedral structure connected

continuously with not the Co–O(1)–Co angle but the Co–O(2)–Co angle of the orthorhombic structure. It is therefore considered that the linear increase in $T_{1/2}$ depends on neither the valence of the metal ion nor the specific surface area, but the crystal structure of the sample. In the rhombohedral structure, both the Co–O distance and the Co–O–Co angle decreased with increases in x. In the orthorhombic structure, however, the average Co–O(2) distance remained nearly constant, and only the Co–O(2)–Co angle decreased with increases in x. From these results, it is considered that the variation in the Co–O distance and the Co–O–Co angle resulted in steric hindrance, and that the decrease in the amount of adsorbed oxygen due to the steric hindrance caused the linear increase in $T_{1/2}$. Zhao and Wachs investigated the selective oxidation of propylene over well-defined supported vanadium oxide catalysts as a function of the oxide support (Al_2O_3, SiO_2, Nb_2O_3, TiO_2, and ZrO_2) [31]. Decreasing the electronegativity of the oxide support cation, the catalytic reactivity qualitatively increased. This reflected the increase in the electron density of the bridging V–O support bond and the bridging oxygen atom's availability for redox reaction. In this system, the electronegativities of the La and Nd are 1.1 and 1.2 [32]. The ionic radii of the La^{3+} ion and the Nd^{3+} ion are 1.36 Å and 1.27 Å , respectively [26]. Because the electronegativity of the A-site of the sample increased and the ionic radius of the A-site decreased with increases in x, it is considered that the electron density of the Co–O bond decreased with increases in x and that $T_{1/2}$ increased linearly with increases in x. This study suggests that control of both the B–O distance and the B–O–B angle is very important to improving the catalytic activity of perovskite-type oxides (ABO_3).

Conclusion

A gel was prepared by adding citric acid to an aqueous solution of lanthanum nitrate hexahydrate, neodymium nitrate hexahydrate, and cobalt acetate tetrahydrate. Perovskite-type $(La_{1-x}Nd_x)CoO_3$ was synthesized by firing the gel at 700 °C in air for 3 h. Although the crystal structure changed from a rhombohedral to an orthorhombic system at $x = 0.4$, the Co–O distance of the rhombohedral structure connected continuously with the average Co–O(2) distance of the orthorhombic structure, and the Co–O–Co angle of the rhombohedral structure and the Co–O(2)–Co angle of the orthorhombic structure were continuous. The linear increase in $T_{1/2}$ was explained by the decrease in the amount of adsorbed oxygen due to steric hindrance.

Acknowledgement This study was supported by the Tanikawa Fund Promotion of Thermal Technology.

References

1. Tejuca LG, Ferro JG, Tascon JMD (1989) Adv Catal 36:237
2. Saracco G, Scibilia G, Iannibello A, Baldi G (1996) Appl Catal B8:229
3. Zanur AJ, Ying J (2000) Nature 403:65
4. García de la Cruz RM, Falcón H, Peña MA, Fierro JLG (2001) Appl Catal B33:45
5. Ciambelli P, Cimino S, Lisi L, Faticanti M, Minelli G, Pettiti I, Porta P (2001) Appl Catal B33:193
6. Yi N, Cao Y, Su Y, Dai WL, Ye HY, Fan KN (2005) J Catal 230:249
7. Royer S, Alamdari H, Duprez D, Kaliaguine S (2005) Appl Catal B58:273
8. Lee SH, Lee JY, Park YM, Wee JH, Lee KY (2006) Catal Today 117:376
9. Seyfi B, Baghalha M, Kazemian H (2009) Chem Eng J 148:306
10. Bialobok B, Trawcznski J, Mista W, Zawadzki M (2007) Appl Catal B72:395
11. Taguchi H, Matsuda D, Nagao M, Tanihata K, Miyamoto Y (1992) J Am Ceram Soc 75:201
12. Taguchi H, Yoshioka H, Matsuda D, Nagao M (1993) J Solid State Chem 104:460
13. Taguchi H, Yoshioka H, Nagao M (1994) J Mater Sci Lett 13:891
14. Taguchi H, Matsu-ura S, Nagao M, Choso T, Tabata K (1997) J Solid State Chem 129:60
15. Taguchi H, Yamada S, Nagao M, Ichikawa Y, Tabata K (2002) Mater Res Bull 37:69
16. Natile MM, Ugel E, Maccato C, Gilisenti A (2007) Appl Catal B72:351
17. Cheng CS, Zhang L, Zhang YJ, Jiang SP (2008) Solid State Ionics 179:282
18. Arai H, Yamada T, Eguchi K, Seiyama T (1986) Appl Catal 26:265
19. Nakamura T, Misono M, Yoneda Y (1982) Bull Chem Soc Jpn 55:394
20. Nitadori T, Kurihara S, Misono M (1986) J Catal 98:221
21. Rosso I, Garrone E, Geobaldo F, Onida B, Saracco G, Specchia V (2001) Appl Catal B30:61
22. Gushee BE, Katz L, Ward R (1957) J Am Chem Soc 79:5601
23. Izumi F, Ikeda T (2000) Mater Sci Forum 321–324:198
24. Raccah PM, Goodenough JB (1967) Phys Rev 155:932
25. Taguchi H (1996) J Solid State Chem 122:297
26. Shannon RD (1976) Acta Cryst A32:751
27. Mastin J, Einarsrud MA, Grande T (2006) Chem Mater 18:1680
28. Liu X, Prewitt CT (1991) J Phys Chem Solid 52:441
29. Haruta M, Yamada N, Kobayashi T, Iijima S (1989) J Catal 115:301
30. Voorhoeve RJH, Johnson DW, Remeika JP, Gallagher PK (1977) Science 195:827
31. Zhao C, Wachs IE (2008) J Catal 257:181
32. Gordy W, Thomas WJO (1956) J Chem Phys 24:439